Asociación Argentina
de Mecánica Computacional

Mecánica Computacional Vol XXVIII, págs. 3191-3205 (artículo completo)
Cristian García Bauza, Pablo Lotito, Lisandro Parente, Marcelo Vénere (Eds.)
Tandil, Argentina, 3-6 Noviembre 2009

DESIGN OF COMPLIANT MECHANISMS THAT EXACTLY FIT A DESIRED SHAPE

Alejandro E. Albanesi, Victor D. Fachinotti and Alberto Cardona

Centro Internacional de Métodos Computacionales en Ingeniería (CIMEC)
INTEC - Universidad Nacional del Litoral
Guemes 3450, 3000 Santa Fe, Argentina
aalbanes@ceride.gov.ar, **http://www.cimec.org.ar**

Keywords: Design of Compliant Mechanisms, Inverse Analysis, Large-Deflection of Beams.

Abstract. A new method for designing compliant mechanisms using an inverse beam model is presented here. Several mechanisms with distributed and concentrated compliance are studied. The proposed inverse model allows to design compliant mechanisms that exactly fulfill the loaded mechanism shape, with lower computational costs compared with other design methods. It is specially suited for problems where an object has to be manipulated by the mechanism with a prescribed contact force, allowing to maximize contact points between the mechanism and the object geometry. In particular, grippers, pliers and brakes are studied here, where results show a perfect matching of the contact shapes.

1 INTRODUCTION

Approximately one decade ago, research and development of a new method to design structures and machine parts began. It consisted in computing the undeformed (reference) configuration knowing the deformed shape of the body and the loads applied. This new method is formally known as an *inverse design problem*, or simply as an *inverse problem*. Inverse methods are useful tools that allow engineers to obtain efficient designs at much lower costs than the ones normally involved in experimental and direct computational design. The inverse method presented here allows an engineer to obtain the precise structures geometry that in work-conditions will acquire a desired pre-specified shape. Classical direct methods simply provide solutions to the physical equations in a natural time-direction. The engineer proposes a first trial for the geometry of the structure, and a direct analysis will provide the deformation of the structure when subject to given external loads. Despite the importance of direct methods, inverse methods constitute a very useful tool that allows engineers to conceive designs in less time and at much lower costs than the ones involved in traditional experimental and direct computational design, and avoid the iterative trial and error approach used many times in the design process. Finite element models for the inverse design of two- and three-dimensional isotropic elastic continuum bodies subjected to large deformations have been proposed by Govindjee and Mihalic (1996), Govindjee and Mihalic (1998) and Yamada (1997) for isotropic behavior, recently extended to orthotropic materials by Fachinotti et al. (2008).

Traditional rigid-body mechanisms consist of rigid links connected at movable joints, and their motion depend on rigid-body translations and/or rotations. Nowadays, many mechanisms are designed to derive some mobility by elastic deformation in one or more elements, so they gain at least some of their mobility from the deflection of flexible members rather than from movable joints only. This latter group is widely known as *compliant mechanisms*. According to how the flexibility is distributed, a compliant mechanism can be classified in two main categories: mechanisms with *distributed compliance*, and mechanisms with *concentrated compliance*. Systems with concentrated compliance are similar to classic rigid link mechanisms, where kinematic joints are replaced with flexible hinges, and so methods conceived to design rigid body mechanisms can be modified and applied to design systems with concentrated compliance. The most popular method to design compliant mechanisms with concentrated compliance is the pseudo-rigid body replacement model, developed by Howell and Midha (1994), and Howell (2001). The purpose of the pseudo-rigid body model provides a simple method to analyze systems that undergo large nonlinear deflections, modelling flexible members as rigid links attached at pin joints, and torsional springs are added to account the force-deflection relationship as links deflect from their initial to final configuration. In short, a compliant mechanism is modeled as an equivalent rigid-link mechanism. On the other hand, mechanisms with distributed compliance are systems where flexibility is evenly distributed, and this avoids stress concentration areas. The mechanisms is modelled as a flexible structure, and so continuum mechanics and structural optimization methods are used to design this kind of mechanisms.

Since most flexible links and flexible hinges are prismatic shaped, and can be modeled as beam-type elements, we present here a *new method to design compliant mechanisms based in an inverse finite element beam model* presented in Albanesi et al. (2008) and Albanesi et al. (2009), as an extension of our previous work in inverse design methods Fachinotti et al. (2008). This is a novel and original method in the field of compliant mechanism, as there is no background of inverse methods among the procedures used to design compliant systems. For the purpose of flexible mechanism analysis and synthesis, a simplified beam theory with a linear-

elastic constitutive relation is adopted. Flexibility effects are introduced by a hypothesis of large displacements and finite rotations, however, it is assumed that the strains which result are small. Finally, it is assumed that beam cross-sections remain straight but can undergo shear strain.

Numerical tests for validation purposes are given, along with applications for the inverse analysis of a compliant mechanism with distributed compliance. The element is being implemented in the MECANO mechanism analysis package.

2 BEAM KINEMATICS

The non-linear beam model relies on the following kinematic hypotheses:

- the beam is straight when unloaded,
- beam cross sections remain plane during deformation, and
- shear deformation of the neutral axis is allowed.

Figure 1: Description of beam kinematics

Let us denote $\mathcal{B}_0$ and $\mathcal{B}$ the undeformed and deformed configuration of the beam, respectively. The position of any point $\boldsymbol{X} \in \mathcal{B}_0$ can be expressed as

$$\boldsymbol{X} = \boldsymbol{X}_0 + \boldsymbol{Y} \tag{1}$$

where $\boldsymbol{X}_0$ is the trace of the neutral axis on the cross section containing point $\boldsymbol{X}$, and $\boldsymbol{Y}$ is the position of $\boldsymbol{X}$ in the cross section,relative to $\boldsymbol{X}_0$. After deformation, the basis in $\mathcal{B}_0$, say, $\{\boldsymbol{E}_1,\boldsymbol{E}_2,\boldsymbol{E}_3\}$ transforms to the basis $\{\boldsymbol{e}_1,\boldsymbol{e}_2,\boldsymbol{e}_3\}$ in $\mathcal{B}$ according to the orthogonal transformation

$$\boldsymbol{e}_i = \boldsymbol{R}\boldsymbol{E}_i \qquad i = 1, 2, 3 \tag{2}$$

where the operator $\boldsymbol{R}$ is formally a linear operator on the abstract three dimensional space and represents the physical rotation between the two basis. Then, the position of any point $\boldsymbol{x} \in \mathcal{B}$ can be expressed as:

$$\boldsymbol{x} = \boldsymbol{x}_0 + \boldsymbol{y} \tag{3}$$

where $\boldsymbol{x}_0$ is the trace of the neutral axis of the deformed beam on the section containing the point $\boldsymbol{x}$, and $\boldsymbol{RY}$ is the position of $\boldsymbol{x}$ in the cross section relative to $\boldsymbol{x}_0$. In the current analysis, where the variables $\boldsymbol{x}_0$ and $\boldsymbol{y}$ that determine $\mathcal{B}$ are assumed to be known, we have to solve a problem for the unknowns $\boldsymbol{X}_0$ and $\boldsymbol{R}$ in order to completely determine $\mathcal{B}_0$.

2.1 Parameterization of rotations

The Cartesian rotational vector $\boldsymbol{\psi}$ is used to parameterize rotations, which is defined as the vector whose direction is that of the rotation axis $\boldsymbol{n}$ and whose length is equal to the amplitude of the rotation ψ:

$$\boldsymbol{\psi} = \boldsymbol{n}\psi \tag{4}$$

Using $\boldsymbol{\psi}$, the rotation operator in three dimensional space is completely determined by means of the Rodrigues' formulae:

$$\boldsymbol{R}(\boldsymbol{\psi}) = \boldsymbol{I} + \frac{\sin\psi}{\psi}\widetilde{\boldsymbol{\psi}} + \frac{1-\cos\psi}{\psi^2}\widetilde{\boldsymbol{\psi}}\widetilde{\boldsymbol{\psi}} \tag{5}$$

where $\boldsymbol{I}$ is the identity matrix and, from now on, $\widetilde{\boldsymbol{u}}$ is the spin operator applied to the vector $\boldsymbol{u}$. Since $\boldsymbol{\psi}$ suffices to completely describe the rotation $\boldsymbol{R}$, let us consider the set of variables $\{\boldsymbol{X}_0, \boldsymbol{\psi}\}$ instead of $\{\boldsymbol{X}_0, \boldsymbol{R}\}$ as the unknown of the current inverse problem.

3 FINITE ELEMENT METHOD

The current "inverse" beam element that represents the deformed configuration $\mathcal{B}$ is a straight, mixed linear-linear finite element whose nodes $\boldsymbol{x}_0^1$ and $\boldsymbol{x}_0^2$ are located at its ends. The unknowns of the inverse problem are approximated as follows:

$$\boldsymbol{X}_0(s) = \varphi_1(s)\boldsymbol{X}_0^1 + \varphi_2(s)\boldsymbol{X}_0^2 \tag{6}$$

$$\boldsymbol{\psi}(s) = \varphi_1(s)\boldsymbol{\psi}^1 + \varphi_2(s)\boldsymbol{\psi}^2 \tag{7}$$

where $\boldsymbol{X}_0^i$ and $\boldsymbol{\psi}^i$ are respectively the unknown values of $\boldsymbol{X}_0$ and $\boldsymbol{\psi}$ at node i, and φ_i is the linear shape function associated to node i. The vector $\boldsymbol{Q}$ of nodal unknowns and the matrix $\boldsymbol{\varphi}$ of shape functions are defined as

$$\boldsymbol{Q} = \begin{bmatrix} \boldsymbol{X}_0^1 \\ \boldsymbol{X}_0^2 \\ \boldsymbol{\psi}^1 \\ \boldsymbol{\psi}^2 \end{bmatrix}, \qquad \boldsymbol{\varphi} = \begin{bmatrix} \varphi_1\boldsymbol{I} & \varphi_2\boldsymbol{I} & \boldsymbol{O} & \boldsymbol{O} \\ \boldsymbol{O} & \boldsymbol{O} & \varphi_1\boldsymbol{I} & \varphi_2\boldsymbol{I} \end{bmatrix} \tag{8}$$

where $\boldsymbol{O}$ is the 3×3 null matrix and $\boldsymbol{I}$ is the 3×3 identity matrix. Then, equations (6) and (7) take the matrix form:

$$\begin{bmatrix} \boldsymbol{X}_0 \\ \boldsymbol{\psi} \end{bmatrix} = \boldsymbol{\varphi}\boldsymbol{Q} \tag{9}$$

4 GOVERNING EQUILIBRIUM EQUATIONS

The equilibrium equations are formulated in the known deformed configuration $\mathcal{B}$. Let us call $\boldsymbol{n}$ and $\boldsymbol{m}$ the resultant force and moment with respect to $\boldsymbol{x}_0$ of the tractions acting over the surface S, and $\bar{\boldsymbol{n}}$ and $\bar{\boldsymbol{m}}$ the external force and moment per unit length at $\boldsymbol{x}$. Assuming static conditions, the equilibrium equations are:

$$\frac{d\boldsymbol{n}}{ds} + \bar{\boldsymbol{n}} = \boldsymbol{0} \tag{10}$$

$$\frac{d\boldsymbol{m}}{ds} + \frac{d\boldsymbol{x}_0}{ds} \times \boldsymbol{n} + \boldsymbol{m} = \boldsymbol{0} \tag{11}$$

Integrating by parts the the weak form of the equilibrium equations (10) and (11) over $\mathcal{B}$, we obtain

$$\int_{\mathcal{B}} \boldsymbol{n} \cdot \left(\frac{d\boldsymbol{w}_1}{ds} + \boldsymbol{i} \times \boldsymbol{w}_2 \right) ds + \int_{\mathcal{B}} \boldsymbol{m} \cdot \frac{d\boldsymbol{w}_2}{ds} = -\int_{\mathcal{B}} \left(\bar{\boldsymbol{n}} \cdot \boldsymbol{w}_1 + \bar{\boldsymbol{m}} \cdot \boldsymbol{w}_2 \right) ds \tag{12}$$

where $\boldsymbol{w}_1$ and $\boldsymbol{w}_2$ are admissible but arbitrary weighting functions. After discretising the above equation following the standard Galerkin finite element method Zienkiewicz and Taylor (2000), the non-linear system of algebraic equations for the unknowns $\boldsymbol{Q}$ is obtained:

$$\boldsymbol{F}_{int}(\boldsymbol{Q}) - \boldsymbol{F}_{ext} = \boldsymbol{0} \tag{13}$$

where $\boldsymbol{F}_{int}$ and $\boldsymbol{F}_{ext}$ are respectively the vectors of internal and external forces, respectively, given by

$$\boldsymbol{F}_{int} = \int_{\mathcal{B}} \boldsymbol{B}^T \boldsymbol{\sigma} ds \tag{14}$$

$$\boldsymbol{F}_{ext} = \int_{\mathcal{B}} \boldsymbol{\varphi}^T \bar{\boldsymbol{t}} ds \tag{15}$$

with

$$\boldsymbol{B} = \begin{bmatrix} \varphi_1' \boldsymbol{I} & \varphi_1 \widetilde{\boldsymbol{i}} & \varphi_2' \boldsymbol{I} & \varphi_2 \widetilde{\boldsymbol{i}} \\ \boldsymbol{O} & \varphi_1' \boldsymbol{I} & \boldsymbol{O} & \varphi_2' \boldsymbol{I} \end{bmatrix}, \qquad \boldsymbol{\sigma} = \begin{bmatrix} \boldsymbol{n} \\ \boldsymbol{m} \end{bmatrix}, \qquad \bar{\boldsymbol{t}} = \begin{bmatrix} \bar{\boldsymbol{n}} \\ \bar{\boldsymbol{m}} \end{bmatrix} \tag{16}$$

where $\varphi_1' = d\varphi_1/ds = -1/L$ and $\varphi_2' = d\varphi_2/ds = 1/L$.

4.1 Constitutive equations

As the material law is necessarily expressed in the material or undeformed frame, we need to introduce the material counterparts of $\boldsymbol{n}$ and $\boldsymbol{m}$:

$$\boldsymbol{N} = \boldsymbol{R}^T \boldsymbol{n} \tag{17}$$

$$\boldsymbol{M} = \boldsymbol{R}^T \boldsymbol{m} \tag{18}$$

Following the constitutive relations used in cardona88, we assume that the material remains in the linear elastic range. Under these hypotheses, the following constitutive equations apply:

$$\boldsymbol{N} = \boldsymbol{C}^N \boldsymbol{\Gamma} \tag{19}$$

$$\boldsymbol{M} = \boldsymbol{C}^M \boldsymbol{K} \tag{20}$$

where $\boldsymbol{\Gamma}$ and $\boldsymbol{K}$ are the material measures of the deformation of the neutral axis and curvature, respectively, and $\boldsymbol{C}^N$ and $\boldsymbol{C}^M$ are the matrices of elastic coefficients.

4.2 Deformation measures in the deformed configuration

Following Géradin and Cardona Géradin and Cardona (2000), we define the deformation of the neutral axis and the curvature as the vectors $\boldsymbol{\gamma}$ and $\boldsymbol{k}$, which are given in the deformed basis by

$$\boldsymbol{\gamma} = \boldsymbol{R}^T \frac{d\boldsymbol{x}_0}{dX_1} - \boldsymbol{E}_1 \tag{21}$$

$$\boldsymbol{k} = \boldsymbol{T} \frac{d\boldsymbol{\psi}}{dX_1} \tag{22}$$

where $\boldsymbol{T}$ is the tangent operator

$$\boldsymbol{T}(\boldsymbol{\psi}) = \boldsymbol{I} + \frac{\cos\psi - 1}{\psi^2} \widetilde{\boldsymbol{\psi}} + \left(1 - \frac{\sin\psi}{\psi}\right) \widetilde{\boldsymbol{\psi}} \widetilde{\boldsymbol{\psi}} \tag{23}$$

(note that $\boldsymbol{T} \to \boldsymbol{I}$ as $\psi \to 0$). The coordinates s and X_1 along the neutral axis in the deformed and undeformed configuration, respectively, are related by

$$\frac{ds}{dX_1} = \frac{L}{L_0} \tag{24}$$

where $L_0 = \|\boldsymbol{X}_0^2 - \boldsymbol{X}_0^1\|$. Then, the *material* measures of the deformation of the neutral axis and curvature, currently referred to the *known deformed frame*, can be computed at the sampling point $s = L/2$, where $\boldsymbol{\Psi} = \boldsymbol{\Psi}_{sp} = (\boldsymbol{\Psi}^1 + \boldsymbol{\Psi}^2)/2$, yields

$$\boldsymbol{\gamma}_{sp} = \frac{L}{L_0}\boldsymbol{R}_{sp}^T\boldsymbol{i} - \frac{\Delta\boldsymbol{X}_0}{L_0} \tag{25}$$

$$\boldsymbol{k}_{sp} = \boldsymbol{T}_{sp}\frac{\Delta\boldsymbol{\psi}}{L_0} \tag{26}$$

with $\boldsymbol{R}_{sp} = \boldsymbol{R}(\boldsymbol{\Psi}_{sp})$ and $\boldsymbol{T}_{sp} = \boldsymbol{T}(\boldsymbol{\Psi}_{sp})$, and where $\Delta\boldsymbol{X}_0 = \boldsymbol{X}_0^2 - \boldsymbol{X}_0^1$ and $\Delta\boldsymbol{\psi} = \boldsymbol{\psi}^2 - \boldsymbol{\psi}^1$. Rotating the material measures (25) and (26) to the material frame, we obtain:

$$\boldsymbol{\Gamma}_{sp} = \boldsymbol{R}_{sp}^T\boldsymbol{\gamma}_{sp} \tag{27}$$

$$\boldsymbol{K}_{sp} = \boldsymbol{R}_{sp}^T\boldsymbol{k}_{sp} \tag{28}$$

4.3 Stress measures in the deformed configuration

The stress measures $s = L/2$ referred to the material frame are computed at the sampling point by invoking the constitutive equations (19) and (20):

$$\boldsymbol{N}_{sp} = \boldsymbol{C}^N\boldsymbol{\Gamma}_{sp} \tag{29}$$

$$\boldsymbol{M}_{sp} = \boldsymbol{C}^M\boldsymbol{K}_{sp} \tag{30}$$

Finally, we rotate these vectors to the deformed frame to obtain:

$$\boldsymbol{n}_{sp} = \boldsymbol{R}_{sp}\boldsymbol{N}_{sp} \tag{31}$$

$$\boldsymbol{m}_{sp} = \boldsymbol{R}_{sp}\boldsymbol{M}_{sp} \tag{32}$$

4.4 Linearization of the discrete equilibrium equations

The non-linear discrete equilibrium equations (13) are solved using the Newton-Raphson method Zienkiewicz and Taylor (2000). At each iteration k, the residual vector $\boldsymbol{F} = \boldsymbol{F}_{int} - \boldsymbol{F}_{ext}$ is approximated using the linear Taylor expansion:

$$\boldsymbol{F}^{(k)} \approx \boldsymbol{F}^{(k-1)} + \boldsymbol{K}^{(k-1)}\Delta\boldsymbol{Q} = \boldsymbol{0} \tag{33}$$

where $\boldsymbol{K}$ is the tangent matrix, defined as

$$\boldsymbol{K} = \frac{d\boldsymbol{F}}{d\boldsymbol{Q}} \tag{34}$$

As aforementioned, only the internal forces are assumed to depend on the unknowns, so that

$$\boldsymbol{K} = \frac{d\boldsymbol{F}_{int}}{d\boldsymbol{Q}} \tag{35}$$

Derivating equation (**??**) with respect to the unknowns $\boldsymbol{Q}$ and taking into account that the matrix $\boldsymbol{B}_{st}$ and the length L of the deformed beam are independent of $\boldsymbol{Q}$, we obtain

$$\boldsymbol{K} = L\boldsymbol{B}_{st}\frac{d\boldsymbol{\sigma}_{st}}{d\boldsymbol{Q}} \tag{36}$$

Then, it only remains to compute the derivatives of the stresses $\boldsymbol{\sigma}_{st}$ with respect to $\boldsymbol{Q}$:

$$\frac{d\boldsymbol{\sigma}_{st}}{d\boldsymbol{Q}} = \begin{bmatrix} \frac{d\boldsymbol{n}_{st}}{d\boldsymbol{Q}} \\ \frac{d\boldsymbol{m}_{st}}{d\boldsymbol{Q}} \end{bmatrix} \tag{37}$$

From now on, let us obviate the subscript sp for notation convenience, keeping in mind however that all the variables are evaluated at the sampling point $s = L/2$.

Let us first compute the variation

$$\delta\boldsymbol{n} = \delta\boldsymbol{R}\boldsymbol{C}^N\boldsymbol{R}^T\boldsymbol{\gamma} + \boldsymbol{R}\boldsymbol{C}^N\delta\boldsymbol{R}^T\boldsymbol{\gamma} + \boldsymbol{R}\boldsymbol{C}^N\boldsymbol{R}^T\delta\boldsymbol{\gamma} \tag{38}$$

From **?**, we know that

$$\delta\boldsymbol{R}\boldsymbol{u} = -\boldsymbol{R}\widetilde{\boldsymbol{u}}\boldsymbol{T}\delta\boldsymbol{\Psi} \tag{39}$$

$$\delta\boldsymbol{R}^T\boldsymbol{u} = \widetilde{\boldsymbol{R}^T\boldsymbol{u}}\boldsymbol{T}\delta\boldsymbol{\Psi} \tag{40}$$

for a given arbitrary vector $\boldsymbol{u}$.

Then, the first term in the r.h.s. of equation (38) can be computed as follows

$$\delta\boldsymbol{R}\boldsymbol{C}^N\boldsymbol{R}^T\boldsymbol{\gamma} = \delta\boldsymbol{R}\boldsymbol{N}\delta\boldsymbol{\Psi} = -\boldsymbol{R}\widetilde{\boldsymbol{N}}\boldsymbol{T}\delta\boldsymbol{\Psi} \tag{41}$$

Computed in a similar way, the second term in the r.h.s. of equation (38) takes the form

$$\boldsymbol{R}\boldsymbol{C}^N\delta\boldsymbol{R}^T\boldsymbol{\gamma} = \boldsymbol{R}\boldsymbol{C}^N\widetilde{\boldsymbol{R}^T\boldsymbol{\gamma}}\delta\boldsymbol{\Psi} = \boldsymbol{R}\boldsymbol{C}^N\widetilde{\boldsymbol{\Gamma}}\delta\boldsymbol{\Psi} \tag{42}$$

The last term in the r.h.s. of (38) requires to compute the variation

$$\delta\boldsymbol{\gamma} = -\frac{\delta L_0}{L_0}\boldsymbol{\gamma} + \frac{L}{L_0}\delta\boldsymbol{R}^T\boldsymbol{i} - \frac{\delta\Delta\boldsymbol{X}_0}{L_0} \tag{43}$$

The variation of L_0 takes the form

$$\delta L_0 = \delta\|\Delta\boldsymbol{X}_0\| = \frac{1}{L_0}\Delta\boldsymbol{X}_0^T\delta\Delta\boldsymbol{X}_0 = \boldsymbol{E}_1^T\delta\Delta\boldsymbol{X}_0 \tag{44}$$

In order to compute the second term in the r.h.s. of equation (43), we invoke equation (40) to obtain

$$\delta\boldsymbol{R}^T\boldsymbol{i} = \widetilde{\boldsymbol{R}^T\boldsymbol{i}}\boldsymbol{T}\delta\boldsymbol{\Psi} \tag{45}$$

Now, we can express the variation of $\boldsymbol{n}$ given by equation (38) in terms of the variations $\delta\boldsymbol{\Psi}$ and $\delta\Delta\boldsymbol{X}_0$ as follows:

$$\delta\boldsymbol{n} = \left(-\boldsymbol{R}\widetilde{\boldsymbol{N}}\boldsymbol{T} + \boldsymbol{R}\boldsymbol{C}^N\widetilde{\boldsymbol{\Gamma}} + \frac{L}{L_0}\boldsymbol{C}^n\widetilde{\boldsymbol{R}^T\boldsymbol{i}}\boldsymbol{T}\right)\delta\boldsymbol{\Psi} - \frac{1}{L_0}\left(\boldsymbol{n}\boldsymbol{E}_1^T + \boldsymbol{C}^n\right)\delta\Delta\boldsymbol{X}_0 \tag{46}$$

This yields:

$$\frac{d\boldsymbol{n}}{d\boldsymbol{Q}} = \left(-\boldsymbol{R}\widetilde{\boldsymbol{N}}\boldsymbol{T} + \boldsymbol{R}\boldsymbol{C}^N\widetilde{\boldsymbol{\Gamma}} + \frac{L}{L_0}\boldsymbol{C}^n\widetilde{\boldsymbol{R}^T\boldsymbol{i}}\boldsymbol{T}\right)\frac{d\boldsymbol{\Psi}}{d\boldsymbol{Q}} - \frac{1}{L_0}\left(\boldsymbol{n}\boldsymbol{E}_1^T + \boldsymbol{C}^n\right)\frac{d\Delta\boldsymbol{X}_0}{d\boldsymbol{Q}} \tag{47}$$

where

$$\frac{d\boldsymbol{\Psi}}{d\boldsymbol{Q}} = \begin{bmatrix} \boldsymbol{O} & \boldsymbol{O} & \frac{1}{2}\boldsymbol{I} & \frac{1}{2}\boldsymbol{I} \end{bmatrix}, \qquad \frac{d\Delta\boldsymbol{X}_0}{d\boldsymbol{Q}} = \begin{bmatrix} -\boldsymbol{I} & \boldsymbol{I} & \boldsymbol{O} & \boldsymbol{O} \end{bmatrix} \tag{48}$$

Let us compute now the variation

$$\delta \boldsymbol{m} = \delta \boldsymbol{R}\boldsymbol{C}^M \boldsymbol{R}^T \boldsymbol{k} + \boldsymbol{R}\boldsymbol{C}^M \delta \boldsymbol{R}^T \boldsymbol{k} + \boldsymbol{R}\boldsymbol{C}^M \boldsymbol{R}^T \delta \boldsymbol{k} \tag{49}$$

Computed in the same way as the first to terms in the r.h.s. of equation (38) for $\delta \boldsymbol{n}$, the first two terms of the r.h.s. of the above equation take the form

$$\delta \boldsymbol{R}\boldsymbol{C}^M \boldsymbol{R}^T \boldsymbol{k} = \delta \boldsymbol{R}\boldsymbol{M}\delta\boldsymbol{\Psi} = -\boldsymbol{R}\widetilde{\boldsymbol{M}}\boldsymbol{T}\delta\boldsymbol{\Psi} \tag{50}$$

$$\boldsymbol{R}\boldsymbol{C}^M \delta \boldsymbol{R}^T \boldsymbol{k} = \boldsymbol{R}\boldsymbol{C}^M \widetilde{\boldsymbol{R}^T \boldsymbol{k}}\delta\boldsymbol{\Psi} = \boldsymbol{R}\boldsymbol{C}^M \widetilde{\boldsymbol{K}}\delta\boldsymbol{\Psi} \tag{51}$$

Then, it remains to compute the variation

$$\delta \boldsymbol{k} = -\frac{1}{L_0}\boldsymbol{k}\delta L_0 + \delta \boldsymbol{T}\frac{\Delta\boldsymbol{\psi}}{L_0} + \boldsymbol{T}\frac{\delta\Delta\boldsymbol{\psi}}{L_0} \tag{52}$$

where

$$\delta \boldsymbol{T}\boldsymbol{\Delta\psi} = \boldsymbol{A}\delta\boldsymbol{\Psi} \tag{53}$$

with

$$\boldsymbol{A} = \left[\begin{array}{ccc} \frac{d\boldsymbol{T}}{d\Psi_1}\Delta\boldsymbol{\psi} & \frac{d\boldsymbol{T}}{d\Psi_2}\Delta\boldsymbol{\psi} & \frac{d\boldsymbol{T}}{d\Psi_3}\Delta\boldsymbol{\psi} \end{array} \right] \tag{54}$$

Now, we can express the variation of $\boldsymbol{m}$ given by equation (49) in terms of the variations $\delta\boldsymbol{\Psi}$, $\delta\Delta\boldsymbol{\Psi}$ and $\delta\Delta\boldsymbol{X}_0$ as follows

$$\delta \boldsymbol{m} = \left(-\boldsymbol{R}\widetilde{\boldsymbol{M}}\boldsymbol{T} + \boldsymbol{R}\boldsymbol{C}^M \widetilde{\boldsymbol{K}} + \frac{1}{L_0}\boldsymbol{C}^m \boldsymbol{A} \right) \delta\boldsymbol{\Psi} - \frac{1}{L_0}\boldsymbol{m}\boldsymbol{E}_1^T \delta\Delta\boldsymbol{X}_0 + \frac{1}{L_0}\boldsymbol{C}^m \boldsymbol{T}\delta\Delta\boldsymbol{\Psi} \tag{55}$$

from which

$$\frac{d\boldsymbol{m}}{d\boldsymbol{Q}} = \left(-\boldsymbol{R}\widetilde{\boldsymbol{M}}\boldsymbol{T} + \boldsymbol{R}\boldsymbol{C}^M \widetilde{\boldsymbol{K}} + \frac{1}{L_0}\boldsymbol{C}^m \boldsymbol{A} \right) \frac{d\boldsymbol{\Psi}}{d\boldsymbol{Q}} - \frac{1}{L_0}\boldsymbol{m}\boldsymbol{E}_1^T \frac{d\Delta\boldsymbol{X}_0}{d\boldsymbol{Q}} + \frac{1}{L_0}\boldsymbol{C}^m \boldsymbol{T}\frac{d\Delta\boldsymbol{\Psi}}{d\boldsymbol{Q}} \tag{56}$$

with $d\boldsymbol{\Psi}/d\boldsymbol{Q}$ and $d\Delta\boldsymbol{X}_0/d\boldsymbol{Q}$ given by equation (48) and

$$\frac{d\boldsymbol{\Delta\Psi}}{d\boldsymbol{Q}} = \left[\begin{array}{cccc} \boldsymbol{O} & \boldsymbol{O} & -\boldsymbol{I} & \boldsymbol{I} \end{array} \right] \tag{57}$$

Equations (47) and (56) completely determines the derivatives of $\boldsymbol{\sigma}$, and hence the tangent matrix $\boldsymbol{K}$.

5 MECHANICAL ADVANTAGE: AMPLIFICATION/DEAMPLIFICATION OF MOTION/FORCE

A compliant mechanisms needs to fulfill at least one of the following tasks, according to its main functional objective:

- Provide a specified output displacement.
- Provide a specified output force.

Either task has to be solved in terms of output level (a prescribed displacement or force has to be provided) or output orientation (a prescribed path or load pose history are the requisite performance criteria). A compliant mechanisms is design to amplify or deamplify the output displacement or force. Because of work conservation reasons, a mechanism that amplifies the output displacement, for instance, will necessarily reduce the force that can be delivered at its output port. Conversely, a mechanisms that is design to amplify the output force will produce less output displacement.

According to Lobontiu (2003), the three components of displacement (in the x, y and z reference axis) at the input node are

$$\begin{aligned} \boldsymbol{u}_{in,x} &= C_{in,x}\boldsymbol{F}_{in,x} \\ \boldsymbol{u}_{in,y} &= C_{in,y}\boldsymbol{F}_{in,y} \\ \boldsymbol{u}_{in,z} &= C_{in,z}\boldsymbol{F}_{in,z} \end{aligned} \tag{58}$$

where $\boldsymbol{u}$ is the displacement, C is the flexibility constant and $\boldsymbol{F}$ in the force applied. Similar reasoning and calculations are used to calculate the displacement components at the output node

$$\begin{aligned} \boldsymbol{u}_{out,x} &= C_{out,x}\boldsymbol{F}_{in,x} \\ \boldsymbol{u}_{out,y} &= C_{out,y}\boldsymbol{F}_{in,y} \\ \boldsymbol{u}_{out,z} &= C_{out,z}\boldsymbol{F}_{in,z} \end{aligned} \tag{59}$$

The mechanical advantage of the mechanism is defined as

$$m.a. = \frac{C_{out,i}}{C_{in,i}} = \frac{\frac{\boldsymbol{u}_{out,i}}{\boldsymbol{F}_{in,i}}}{\frac{\boldsymbol{u}_{in,i}}{\boldsymbol{F}_{in,i}}} = \frac{\boldsymbol{u}_{out,i}}{\boldsymbol{u}_{in,i}} \tag{60}$$

which is the ratio of between the output and input displacements. An alternative definition of mechanical advantage, according to Howell (2001), is the ratio of the output force/torque to the input force/torque required. The mechanical advantage may be calculated assuming that power is conserved between the input and the output and that the system is in static equilibrium. In this case, the mechanical advantage is defined as the ratio of the output force $\boldsymbol{F}_{out}$ to the input force $\boldsymbol{F}_{in}$

$$m.a. = \frac{\boldsymbol{F}_{out}}{\boldsymbol{F}_{in}} \tag{61}$$

6 TESTS AND APPLICATIONS

6.1 Inverse Design of a Compliant Gripper

We analyze the compliant gripper proposed by Lan and Cheng (2007), where the final deformed shape and force applied are design parameters, and the undeformed shape is to be found. The gripper is made of flexible beam segments with distributed compliance, where the cross-section height and width are $h = 5$ mm and $b = 10$ mm respectively, and it is fixed at both free ends. The gripper is acted upon an input force $P = 12$ N, and its made of Polypropylene. The material data is shown in Table 1. In the aforementioned work, the problem is solved using intrinsic functions to parameterize the topology and the generalized multiple shooting method

Elastic modulus	Poisson ratio	Tensile shear strength
E = 1.4 $\times 10^3$ N/mm^2	$\nu = 0.35$	$\sigma_{shear} = 34$ N/mm^2

Table 1: Material properties of Polypropylene

(GMSM) is used to analyze the deflection of the mechanisms, integrated to an optimization scheme in order to accomplish design constraints.

This problem was reproduced with much lower computational costs using the inverse beam model. Figure (2) displays the deformed and undeformed shapes, where points **A** and **B** are the fixations of the model and **P** is the input force. The objective of the gripper is to grab an object of a certain size and shape (design requirements) when the gripper is acted upon. The topology was discretized using 90 finite elements, and the analysis was computed in 14 iterations. The model also allows to perfectly match the shape of the gripper and the object, and this leads to maximize the contact points between the gripper and the object. This example shows the direct application of the model in a synthesis task, where we start from the design requirements in order to obtain a final design.

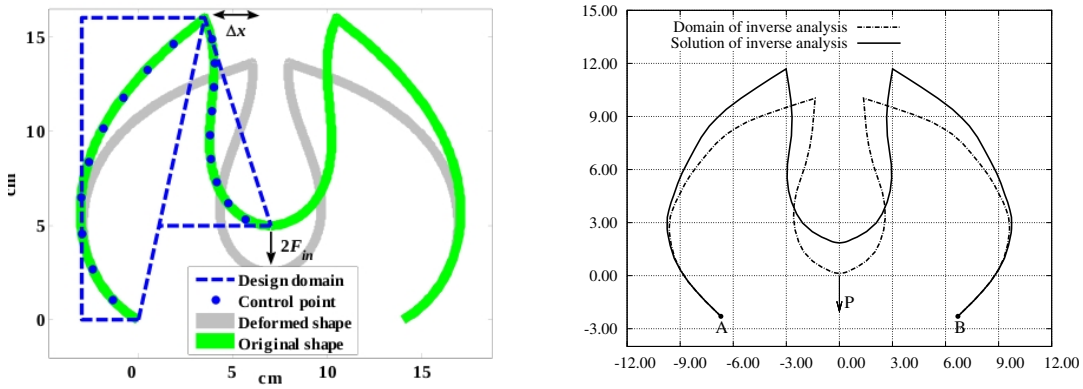

Figure 2: Compliant gripper solved by Lan and Cheng (2007) (left), and by the inverse beam model (right)

We are going to calculate the mechanical advantage for different alternative designs of the gripper, all with the same deformed configuration. First, we calculate the mechanical advantage of the gripper with the 12 N input force proposed by Lan and Cheng (2007). The norm of the displacement will be used. At the input node, the norm of displacement is $\boldsymbol{u}_{in,norm} = 10.612$ mm. The gripper has two output edges. The geometry is symmetric, and the displacement at both the left, and right output nodes is the same. The norm of the output displacement is the double of one of this outputs: $\boldsymbol{u}_{out,norm} = 28.70$ mm. The mechanical advantage is $m.a. = 2.7046$.

Now, lets try different design parameters and evaluate the mechanical advantage variation. In the inverse model, the deformed configuration is the only fixed design parameter. Cross-sections, input force and/or displacements, and material are the design parameter that can be changed in order to obtain a feasible design, with the expected mechanical advantage. For example, if the cross section height is reduced to $h = 3$ mm, the input and output displacements are $\boldsymbol{u}_{in,norm} = 47.631$ mm and $\boldsymbol{u}_{out,norm} = 119.28$ mm respectively, and the mechanical advantage results $m.a. = 2.5043$. This reduction in the mechanical advantage is almost intuitive, in the sense that the structure now has a higher degree of compliance and deformation is distributed more evenly, so the displacement of input and output nodes become similar in modulus.

Finally, if the cross section height is increased to $h = 7$ mm, the input and output displacements are $\boldsymbol{u}_{in,norm} = 3.9285$ mm and $\boldsymbol{u}_{out,norm} = 10.659$ mm respectively, and the mechanical

advantage is $m.a. = 2.7132$. As the cross section height is increased, the degree of compliance is reduced. Its a case of concentrated flexibility, as there are regions of the structure where the deformation is lower than in other points (deformation of soft-curved edges is higher than in sharp-curved edges as the rigidity in the latter case is increased). This is an example of three compliant mechanisms with the same deformed configuration (design requirement) but with different mechanical advantages, and the results are summarized in Table 2.

Section height	Section width	$\boldsymbol{u}_{in,norm}$	$\boldsymbol{u}_{out,norm}$	Mechanical advantage
h = 3 mm	b = 10 mm	3.930 mm	10.660 mm	m.a. = 2.5043
h = 5 mm	b = 10 mm	47.631 mm	119.28 mm	m.a. = 2.7046
h = 7 mm	b = 10 mm	10.612 mm	28.700 mm	m.a. = 2.7132

Table 2: Mechanical advantage vs. cross-section height for the gripper with a 12 N input force

6.2 Inverse Analysis of a Compliant Centrifugal Clutch

In this application, we want to determine the manufacture shape of a compliant centrifugal clutch that connects two concentric shafts, such that its deformed shape causes the clutch shoes to engage the friction surface of the outer drum under the effect of centrifugal loads. An outstanding feature of the inverse model is that the clutch can be directly designed to engage at a certain speed (revolutions per minute or RPM), which is in general at or near the torque peak of the engine. Another important advantage is that the deformed geometry of the clutch will match exactly the geometry of the drum, and this leads to ensure a smooth distribution of the contact force in both surfaces. The model reproduced here was presented by Crane (1999), and its called the S type of centrifugal clutch, figure (3). Among the different compliant centrifugal clutches, this model has several advantages, such as reducing stress concentration, and an even wear distribution in the contact surfaces.

Numerous design requirements can be simultaneously satisfied with the inverse model. For instance, slipping of the clutch and the outer drum with a specified friction force. In several applications where a two-stroke internal combustion engine is used as a power source, some slipping of the clutch is needed in order to keep the shaft speed above a certain RPM number, near the torque peak of the engine. This is the case in many garden tools like lawn-motors, chainsaws, and even some small motorcycles.

Elastic modulus	Shear modulus	Tensile shear strength
E = 69 $\times 10^3$ N/mm^2	G = 25 N/mm^2	$\rho = 2.7 \times 10^{-6}$ Kg/mm^3

Table 3: Material properties of Aluminum alloy

Following the procedure and parameters found in Crane (1999), we will use the inverse model to design a centrifugal S clutch for a small chain-saw, with a 30% slipping coeffient and a friction force (total) $\boldsymbol{F} = 15$ N at 1500 RPM. Its made of an aluminum alloy, and the material data is shown in Table 3. The clutch shoes are made of flexible beam segments with distributed compliance. The slipping percentage means that the drum is rotating at 1500 RPM, but inner part of the clutch (arms and shoes) that is attached to the engine's shaft is rotating 30% faster, at 1950 RPM, in order to keep the engine in the high torque range. This rotation speed difference

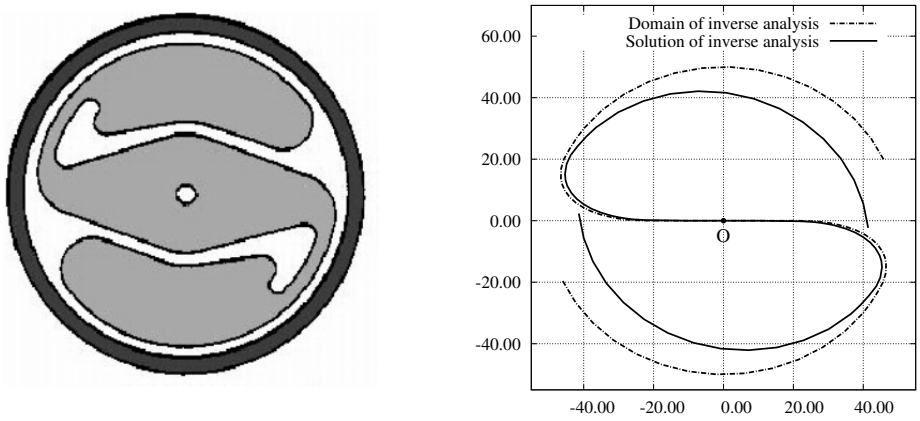

Figure 3: The S type of centrifugal clutch (left), and the solution of the design problem (right)

is caused by the slipping phenomena. The friction force is computed by

$$\boldsymbol{F} = \mu\, \boldsymbol{N} \tag{62}$$

The forces on the clutch arm can be summed and solved for the frictional force. Each arm of the clutch should apply a friction force $\boldsymbol{F}_i = 7.50$ N in order to achieve the total friction force to be transmitted. The average friction coefficient of the rubber surface, in dry condition, is $\mu = 0.7$. According to equation (62), the centrifugal force $\boldsymbol{N}$ should be

$$\boldsymbol{N} = \frac{\boldsymbol{F}}{\mu} = \frac{7.50 \text{ N}}{0.7} = 10.70 \text{ N} \tag{63}$$

The design parameters are the deformed geometry, the rotational velocity 1950 RPM, and the centrifugal force $\boldsymbol{N} = 10.70$ N. At this point, its necessary to relate the angular acceleration and the centrifugal force

$$\boldsymbol{N} = m\omega^2 \boldsymbol{r} \tag{64}$$

where m is the mass of a single clutch arm, ω is the rotational frequency measured in Hz, and $\boldsymbol{r}$ is the radius of rotation. As the radius of rotation is one of the design parameters, the mass m of the arms is to be calculated with the material density, the cross-section area and the arm's length (volume of material). At 1950 RPM the rotational frequency is $\omega = 32.50$ Hz, the radius of the clutch is $\boldsymbol{r} = 55$ mm, and the mass of the shoe results

$$m = \frac{\boldsymbol{N}}{\omega^2 \boldsymbol{r}} = \frac{10.50 \text{ N}}{32.50 \text{ Hz}^2\ 0.055 \text{ m}} = 0.184 \text{ Kg} \tag{65}$$

According to the density ρ, the volume of material needed is 6.8×10^4 mm^3, which results in a cross-section width $b = 39.5$ mm. With this data, the inverse model will provide us the manufacture shape of the clutch, son when its rotating at 1950 RPM, the total friction force driving the drum will be $\boldsymbol{F} = 15$ N. The topology was discretized using 64 finite elements, and the analysis was computed in 16 iterations. The solution is shown in figure (3), where **O** is the axis of rotation and the manufacture shape is represented by the solid line.

6.2.1 Inverse design of a compliant wiper blade

We analyze the compliant wiper blade proposed by Jung et al. (2009). The manufacture shape of a compliant blade is to be found, such that when its pressed against the windshield and obtains its deformed shape, complies with the proper contact pressure distribution and contact angle between wiper and windshield. These are the most important factors and have significant effect on the wiping performance of the blade. If the contact pressure is non-uniformly distributed along the blade, the blade may be detached from the windshield. So, some region of the windshield cannot be cleaned and the blade may be worn partially. On the other hand, if the contact pressure is too high or too low, noise is made and the high frequency vibration phenomena called chattering occurs. Therefore, the major design parameters of the flat type blade are the material property, initial curvature and the shape of the cross-section. These design parameters should be considered seriously at the design stage and optimized to improve the wiping performance. Compliant blades have several advantages over conventional blades, figure (4), because in the latter case the contact pressure between the blade and windshield is distributed non-uniformly since the force by the leaf spring is concentrated on the point where the leaf spring is connected to the rubber. Thus, some parts of the blade may be detached from the windshield, and some regions of windshield cannot be cleaned.

Figure 4: Conventional wiper blade (left), and a compliant wiper blade (right)

The flat blade is composed by a main curved beam (that deforms and produces the pressure against the windshield, and its responsible for the shape change of the blades), and by two rubber parts, one underneath the beam (the wiper part), and another on top of the beam for aerodynamic purposes. The design parameters are then the windshield shape (the final deformed configuration of the blades beam, in order to make a perfect fit with the windshield), and the contact pressure between the blade and windshield. In Jung et al. (2009), the blade is divided into 3 different parts: rigid, small deformation and large deformation bodies in order to find its bending characteristics through FE analysis. The small deformation body is modeled using a modal coordinate formulation, and the large deformation body is modeled using an absolute nodal coordinate formulation.

Again, this problem was reproduced with much lower computational costs using the inverse beam model. The main self-porting part of the blade is made of polypropylene and modelled as flexible beam segments with distributed compliance. As in the gripper example, material data is shown in Table 1. The objective of the inverse analysis is to find the manufacture shape of the self-porting part, such that when its pressed against the windshield by the wiper arm, the resulting geometry and contact pressure maximize the wiping performance. The cross-section height and width are $h = 5$ mm and $b = 15$ mm respectively, and it is fixed at its middle position. The blade deformed configuration is a 7 degree arc sector of a circle with a 5.0 m radius or curvature, and was discretized using 23 finite elements, and the analysis was computed in 11 iterations.

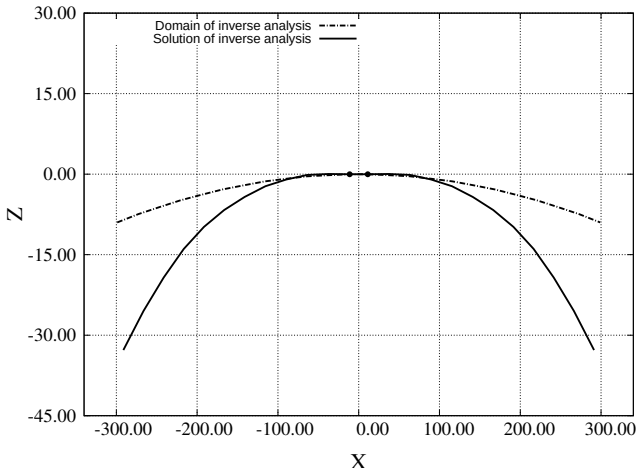

Figure 5: Compliant wiper blade design

7 THE INVERSE MODEL AS A TOOL TO DESIGN MECHANISMS: ADVANTAGES AND/OR DISADVANTAGES

In the previous section we have presented numerical applications of the inverse beam model applied to compliant mechanisms design. It is convenient to make some final comments of the inconvenients found in the design process while using inverse analysis. The first draw-back is that in a few cases, intersections of beam elements exists in the undeformed configuration, even thought the inverse analysis started from a valid deformed geometry, figure (6). This type of problems also lead to a trial and error process (changing the beam cross-section, or the material), until the intersection dissapears. Figures X and X show two non-valid results obtained using the inverse analysis. A proposed solution to this problem would be to implement a simple contact problem of the type node-to-segment with penalty Puso and Laursen (2004) and soft contact algorithms with friction for 3D beams Litewka (2007), in order to impose restrictions of the solution and eliminate unfeasible designs.

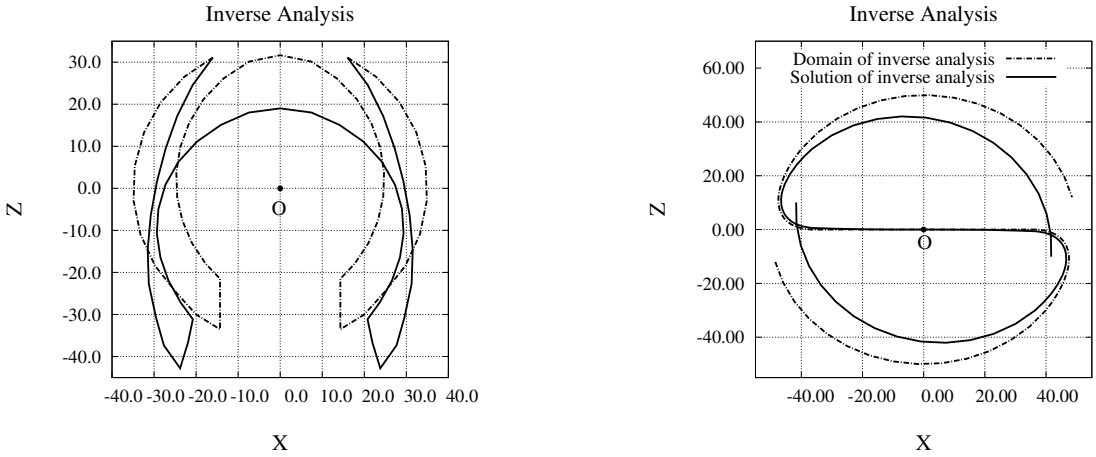

Figure 6: Non-valid results for the compliant gripper (left) and compliant clutch (right)

Another draw-back is that the evolution of the model, as it evolves between the deformed to the undeformed configuration is unknown. This could also lead to unfeasible designs, because at a certain iteration, a beam element may fall outside of the desired design domain.

For instance, in the compliant clutch example, we may encounter a case where the tip of the clutch shoes engage contact with the outer drum at a low RPM number, as it evolves from the closed-undeformed configuration to the deformed configuration.

ACKNOWLEDGEMENTS

The authors gratefully acknowledge the financial support from the Consejo Nacional de Investigaciones Científicas y Técnicas (CONICET). Also, we kindly thank Martin A. Pucheta for his guidance and contributions in compliant mechanism design.

REFERENCES

A. Albanesi, V. Fachinotti, and A. Cardona. Finite element modelling of inverse large-displacement beams. *Asociacin Argentina de Mecnica Computacional*, 27:1049–1061, 2008.

A. Albanesi, V. Fachinotti, and A. Cardona. Inverse analysis of large-displacement beams. *MULTIBODY DYNAMICS 2009, ECCOMAS Thematic Conference*, 2009.

N. Crane. *PhD Thesis. Compliant Centrifugal Clutches: Design, Analysis and Testing*. Brigham Young University, 1999.

V. Fachinotti, A. Cardona, and P. Jetteur. Finite element modelling of inverse design problems in large deformations anisotropic hyperelasticity. *International Journal for Numerical Methods in Engineering*, 74:894–910, 2008.

M. Géradin and A. Cardona. *Flexible Multibody Dynamics. A Finite Element Approach*. John Wiley & Sons, 2000.

S Govindjee and P. A. Mihalic. Computational methods for inverse finite elastostatics. *Computer Methods in Applied Mechanics and Engineering*, 136:47–57, 1996.

S Govindjee and P. A. Mihalic. Computational methods for inverse deformations in quasi-incompressible finite elasticity. *International Journal for Numerical Methods in Engineering*, 43:821–838, 1998.

L. L. Howell. *Compliant Mechanisms*. John Wiley & Sons, 2001.

L. L. Howell and A. Midha. A method for the design of compliant mechanisms with small-length flexural pivots. *Structural Engineering and Mechanics*, 290:280–290, 1994.

S. P. Jung, T. W. Park, D. H. Jung, and W. S. Chung. Two dimensoinal flexible dynamic analysis of the wiper blade. *MULTIBODY DYNAMICS 2009, ECCOMAS Thematic Conference*, 2009.

C-C. Lan and Y-J. Cheng. Distributed shape optimization of compliant mechanisms using intrinsic functions. *Proceedings of ASME International Design Engineering Technical Conferences Computer and Engineering Conference*, 2007.

P. Litewka. Smooth frictional contact between beams in 3d. *Computational Contact Mechanics*, pages 157–176, 2007.

N. Lobontiu. *Compliant Mechanisms. Design of Flexure Hinges*. CRC Press, 2003.

M. A. Puso and T. A. Laursen. A mortar segment-to-segment contact method for large deformation solid mechanics. *Computer Methods in Applied Mechanics and Engineering*, 193: 601–629, 2004.

T. Yamada. Finite element procedure of initial shape determination for hyperelasticity. *Structural Engineering and Mechanics*, 436:173–183, 1997.

O. C. Zienkiewicz and R. L. Taylor. *The finite element method*, volume 2. Butterworth-Heinemann, London, 2000.